Environmental Science and Pollution Research (2021) 28:57073–57089
https://doi.org/10.1007/s11356-021-14638-3

RESEARCH ARTICLE

Efficient removal and recovery of uranium from industrial radioactive wastewaters using functionalized activated carbon powder derived from zirconium carbide process waste

Majid Mohammad Nezhad[1] · Abolfazl Semnani[1] · Nahid Tavakkoli[2] · Mahboube Shirani[3]

Received: 22 February 2021 / Accepted: 26 May 2021 / Published online: 3 June 2021

Abstract

Development of efficient sorbents for selective removing and recovery of uranium from radioactive wastewaters is highly important in nuclear fuel industries from the standpoint of resource sustainability and environmental safety issues. In this study, carbon powder waste was modified by various chemical activating agents under atmosphere of nitrogen gas at 725 °C to prepare an efficient sorbent for removal and recovery of uranium ions from radioactive wastewaters of nuclear fuel conversion facility. Activation of the carbon powder with KOH, among different activators, provided maximum porosity and surface area. The activated samples were modified by reacting with ammonium persulfate in sulfuric acid solution to generate surface functional groups. The synthetized sorbents were characterized with FT-IR, XRD, BET, and SEM-EDS techniques. The effects of solution pH, contact time, initial uranium concentration, and temperature on the sorption capacity of the sorbent with respect to U(VI) from wastewater were investigated by batch method, followed by optimizing the effect of influential parameters by experimental design using central composite design. The sorption of UO_2^{2+} ions on the sorbents follows the Langmuir isotherm and pseudo-second-order kinetic models. Maximum sorption capacity for U(VI) was 192.31 mg g^{-1} of the modified sorbent at 35 °C. Thermodynamic data showed that sorption of U(VI) on the sorbent was through endothermic and spontaneous processes. The sorption studies on radioactive effluents of the nuclear industry demonstrated that the modified sorbent had a favorable selectivity for uranium removal in the presence of several other metal ions.

Keywords Uranium recovery · Modified carbon powder · Chemical modification · Nuclear wastewater · Waste carbon

Introduction

Nuclear power as a promising renewable source of clean energy has gained enormous attention in recent years which has led to incredible development in all over the world (Ishag et al. 2020). However, the main obstacle is radioactive pollution with irreparable harm to the environment which is also considered a fatal health risk (Song et al. 2019). Uranium is the essential raw material in nuclear industry and also is enumerated as the most perilous radionuclide pollutant owing to its long lifetime and dominant chemical and biological toxicity and radioactivity. Long-term exposure and bioaccumulation of uranium can eventuate to irreversible organism detriment, cancer, muscle cramp, liver damage, and nephritis (Liu et al. 2021a). Uranium is discharged into the environment in hexavalent form, mostly as uranyl ion (UO_2^{2+}), through the radioactive wastewater.

One of the noticeably restricting factors in the nuclear industry is releasing massive amounts of U(VI)-polluted wastewater or effluent into the environment which can result in significant amounts of uranium entrance into the food chain causing harmful biological effects in humans and other living organisms. Remediation of radioactive wastewater not only prevents the environmental and ecological pollution but also

Responsible Editor: Tito Roberto Cadaval Jr

✉ Abolfazl Semnani
a.semnani1341@gmail.com

✉ Mahboube Shirani
m.shirani@ujiroft.ac.ir

[1] Department of Chemistry, Faculty of Science, Shahrekord University, P.O. Box 115, Shahrekord, Iran

[2] Chemistry Department, Payame Noor University, Tehran 19395-4697, Islamic Republic of Iran

[3] Department of Chemistry, Faculty of Science, University of Jiroft, P. O. Box, Jiroft 7867161167, Iran

can result in recovery of considerable amounts of uranium to be reused in nuclear process cycle. Various techniques including adsorption (Zhuang and Wang 2020), ion exchange (Cheng et al. 2019), photocatalytic reduction (Deng et al. 2019), membrane processing (Ghasemi Torkabad et al. 2017), and solvent extraction (Mokhine et al. 2020) have been reported for uranium removal from wastewaters. Among them, methods based on adsorption of uranium seems to be a good choice due to its simplicity, rapidity, versatility, and convenience. For removal of uranium through adsorption process, many adsorbents such as metal organic frameworks (MOFs) (Guo et al. 2019), magnetic nanocomposites (Huang et al. 2020), molecularly imprinted polymers (Elsayed et al. 2021), and covalent organic frameworks (COFs) (Li et al. 2020b) have been applied. Moreover, various modified commercial sorbents including zeolite (Liu et al. 2021b), alumina (Chung et al. 2018), bentonite (Zahran et al. 2019), kaolinite (Taha et al. 2018), and carbonaceous materials (activated carbon, carbon nanotubes) (Wang et al. 2020; Yi et al. 2020; Zhang et al. 2018) have been also reported. However, nontoxicity, affordability, and accessibility of the raw materials, and ease of the operational process are some of the most important features of an ideal adsorbent particularly in industrial scales (Zhang et al. 2020b). Among all the reported adsorbent, carbonaceous materials especially active carbon (AC) can be considered the most accessible components which have been satisfactorily applied for uranium removal. Active carbon is one of the most versatile carbonaceous sorbents due to its significant properties such as high mechanical, thermal, and chemical stability, porous structure, low cost, and facile accessibility (Wu et al. 2020). Although AC has been widely applied for heavy metals removal (Mullick et al. 2018; Ribeiro et al. 2018), the main drawback of untreated AC is its low selectivity owing to adsorption of a large category of compounds. Moreover, the absence of suitable functional groups on raw (commercial) AC causes low adsorption kinetics and low adsorption capacity, which makes it unsuitable as a universal sorbent for removal of inorganic ions such as U(VI) (Duan et al. 2021). Various functional groups such as magnetic iron oxide-urea (Mahmoud et al. 2017), polyethylenimine (Saleh et al. 2017), thioacetamide (Tan et al. 2018), magnesium hydroxide impregnation (Saputra et al. 2019), and amidoxime (Lu et al. 2017) have been reported to improve the adsorption ability and selectivity of AC. Meanwhile, proper functional groups that modify the AC surface bring the advantages of large specific surface area (Brunauer-Emmett-Teller (BET)), high adsorption capacity, high selectivity, low cost, ease of recovery, and low consumption of chemical materials and toxic organic solvents.

The purpose of this study is modification of carbon powder waste (CPW) from zirconium carbide processing industry to prepare an adsorbent with large surface area and high capacity for efficient removal and recovery of uranium from radioactive wastewaters of nuclear fuel conversion factory. To this aim, CPW is first activated by various chemical reagents such as $ZnCl_2$, KOH, or $FeCl_3$ to find out the best activator which provides the best characteristics including surface area, pore volume, and iodine adsorption number. The resulting AC is subjected to further modification by treatment with ammonium persulfate, $(NH_4)_2S_2O_8$ (APS), to generate surface functional groups which are expected to significantly improve adsorption capacity and selectivity of the sorbent. In the next step, the performance of the sorbent for adsorption of uranium is investigated and the effects of different influential parameters including contact time, initial uranium concentration, solution pH, and sorption temperature are optimized by experimental design using central composite design (CCD) technique and Minitab-17 software. Finally, the regeneration performance of the sorbent was evaluated through consecutive adsorption and desorption cycles for recovery of the adsorbed uranium and reuse the sorbent. The significance of the present work resides on the fact that a waste carbon material which is a potential pollutant is converted to an effective sorbent for removal of the highly toxic radioactive uranium from wastewaters. The sorbent is a promising alternative to other separation processes such as those based on expensive ion exchange resins or on the use of highly toxic and environmentally hazardous organic solvents.

Experimental

Chemicals

All the reagents in this study were of analytical grade with the highest purity available. Ferric chloride (≥ 98.0 %, Across), zinc chloride (≥98%, Merck), and potassium hydroxide (≥ 85.0 %, Merck) were applied as the activating agents. APS (98%, Merck) was used for functionalization of the sorbents. Stock solution of U(VI) (1000 mg L^{-1} U) was prepared from uranyl nitrate hexahydrate (98%, Merck) by dissolving 2.11 g in 1 L of distilled water. The working solutions (25–125 mg L^{-1}) were prepared daily by dilution of the stock solution. Carbon powder waste from zirconium carbide processing industry with particle size of 5 to 53 μm was used as the raw material for preparation of the sorbents.

Instrumentation

The morphological characterizations of the precursor and sorbents were carried out on a scanning electron microscope (SEM, COXEM) equipped with an energy dispersive spectrometer (EDS, IXRF-model 550i analyzer). The X-ray diffraction patterns of the precursor and sorbents were obtained with an X-ray diffraction (XRD) apparatus (XRD, STOE) using Cu-Kα radiation at λ= 1.54056 Å. The specific surface

areas and pore diameters were evaluated from N_2 adsorption-desorption isotherms at −196 °C and Brunauer-Emmett-Teller (BET) analysis according to ISO 9277-2010 using a sorptometer (Costech, Model 1042) (Brunauer et al. 1938). FT-IR spectroscopy (Perkin Elmer Spectrum 100, USA) was used to identify the functional groups using the potassium bromide (KBr) pellet method. The volatile matter and ash content of all the samples were determined by the ASTM D5832-98 and ASTM D2866-94 standard methods using TGA instrument (model 601 Leco). Elemental analyses (C, N, H, O, and S) of the raw material and the prepared sorbents were accomplished using a CHNOS analyzer (Elementar Vario EL III). The pH at the point of zero charge (pH_{pzc}) of the sorbents was obtained using a simple mass titration method (Leon y Leon et al. 1992). Iodine number of the sorbents was obtained according to ASTM D 4607-99. To assess the number of oxygen functional groups and acidic or basic properties of the sorbent, the Boehm titration method was used (Bandosz et al. 1992; Boehm 2002). Inductively coupled plasma atomic emission spectrometry (ICP-OES, GBC, model Integra XL) was applied for evaluation of U(VI) concentrations. A digital pH meter (model 746 Metrohm) was used for pH measurements.

Real sample preparation

The working samples (real samples) were collected from the radioactive wastewater output of the nuclear fuel factory of Isfahan. The wastewater samples were filtered and then their pH was adjusted to 2 using hydrochloric acid (0.2 mol L^{-1}). The prepared samples were treated according to the given procedure.

Activation process of CPW

Before the activation process, CPW was rinsed with 5% (v/v) HCl solution and then washed with hot and cold distilled water several times to remove any possible impurities. The obtained sorbent was dried at 110 °C for 8 h. The chemical activation was carried using KOH, $ZnCl_2$, and $FeCl_3$ as the activating agents. The activation process consists of two steps. In the first step, 6 g each of KOH, $ZnCl_2$, and $FeCl_3$ was dissolved in 50 mL of distilled water and then 2.0 g of CPW was added (activator to precursor weight ratio of 3:1) and thoroughly mixed (Ghanim et al. 2020). The mixture was stirred at 100 rpm and 60 °C for 10 h. The saturated CPW was filtered and dried at 110 °C for 8 h. In the second step, the resulting CPW was loaded into a crucible and placed in a horizontal cylindrical reactor in a tube furnace (10 cm i.d. and 50 cm length). The activation process was accomplished under nitrogen at flow rate of 100 mL min^{-1} by heating the samples from 25 °C to the activation temperature of 725 °C at a heating rate of 10 °C min^{-1}, followed by maintaining at this temperature under nitrogen flow for 2 h. At the end of the activation time, the samples were cooled down to room temperature under nitrogen flow. Then, the prepared sorbents were washed by stirring with 100 mL HCl (1 mol L^{-1}) or NaOH (1 mol L^{-1}) solution (depending on the type of activator) for 20 min at 70 °C. The samples, after filtration, were washed with hot and then cold distilled water to eliminate the soluble salts and ions such as potassium, iron, zinc, and other impurities. The washing process was continued until the pH value of the filtrate reached 6.5–7.5. Finally, the activated sorbents (A-CPW) were dried at 110 °C for 8 h in vacuum oven, and after cooling they were stored in closed plastic containers to protect them from ambient moisture.

Modification process of A-CPW

In order to improve the adsorption capacity and efficiency of the prepared A-CPW, the sorbent surface was modified with oxygen functional groups. Extensive studies have shown that the increase in sorption capacity and selectivity of the sorbent after chemical modification by APS is due to the increased number of active binding sites and formation of new functional groups such as carboxylic (-COOH) and hydroxylic (-OH) on the sorbent surface (Marciniak et al. 2018; Qu et al. 2021). The resulting oxygen functional groups increase hydrophilicity of the sorbent surface, causing improved electivity and efficiency of the sorbent. Therefore, in this work, the sorbent was oxidized with APS as the oxidant reagent. First, the A-CPW was treated with 15% (v/v) HCl solution for 10 h at 50 °C. Then, 3 g of the sorbent was added to 100 mL solution of 1.8 mol L^{-1} APS in 2.0 mol L^{-1} H_2SO_4 solution and the mixture was stirred for 12 h at 30 °C. After that, the mixture was filtered and washed with distilled water several times until the washing water became neutral (pH ~ 6.0–7.0). The final sorbent (A-CPW-COOH/ox-A-CPW) was kept in a vacuum oven at 110 °C for 7 h. The number of functional surface groups was estimated using the Boehm titration approach (Boehm 2002).

Determination of pH at the point of zero charge

The pH at the point of zero charge (pH_{PZC}) was evaluated by the mass titration method. To determine pH_{PZC} of the A-CPW and A-CPW-COOH, 0.5 g of sorbents was weighed out and placed in 50-mL glass flasks and mixed with 25 mL of 0.01 M NaCl solution. Then, the pH values of the suspensions were adjusted at 2.06, 3.13, 5.25, 6.37, 7.83, 9.58, and 10.85. The suspensions were kept at 25°C with constant stirring (100 rpm) for 24 h. Then, the final pH was measured in each solution using a digital pH meter (model 746 Metrohm). The change of pH (ΔpH) during equilibration was calculated, and the pHpzc was identified as the initial pH with minimum

ΔpH from the pH initial versus ΔpH plot. (The pHpzc is the point where $pH_{initial}$ - pH_{final} = 0.)

The batch adsorption experiments

The accurate amount of the sorbent (50 mg) was added into the beakers containing 100 mL of U(VI) solutions with various concentrations of 25 to 125 mg L^{-1}. The pH of initial solutions was adjusted from 2.5 to 8.5 by 0.1 mol L^{-1} NaOH or HNO_3 solution. Then, the parameters of temperature and time were determined according to the experimental design. The mixture was stirred at a constant temperature with the rate of 150 rpm for 130 min using mechanical stirrer. After that, the mixtures were filtered by filter paper (Whatman no. 42) and the concentration of uranium ions was determined using ICP-OES at λ= 385.958 nm. The values of influential parameters including solution pH, initial concentration, contact time, and temperature were set according to the CCD experimental design. The schematic of batch process for uranium ion removal is presented in Scheme 1.

Experimental design

Response surface methodology (RSM) as one of the most powerful techniques in factorial designs is a collection of statistical and mathematical methods which is employed for the approximation and optimization of stochastic models (Naderi et al. 2018). The effects of prominent parameters including temperature (T) (10, 20, 30, 40, and 50 °C), contact time (t) (10, 60, 110, 160, and 210 min), initial concentration (C_0) (25, 50, 75, 100, and 125 mg L^{-1}), and pH of the solution (2.5, 4.0, 5.5, 7.0, and 8.5) with a certain amount of sorbent (50 mg) on the adsorption of U (VI) were explored using the central composite design (CCD) as a partial factorial design. The CCD is mostly applied to design the second-order model methods. To this aim, Minitab software version 17.0 was used to design and assess the variables at five levels on the responses. To deliberate the precision of the process, four replicates at the center of the design were used; and also to minimize the influence of the studied factors, the experiments were randomized.

Batch sorption studies

To obtain the sorption capacity (q_e (mg g^{-1})) of the sorbent and the removal efficiency (R %) of U(VI) ions from the wastewater, the following equations were used:

$$q_e = V(C_0 - C_e)/m \quad (1)$$

$$R\% = ((C_0 - C_e)/C_0) \times 100 \quad (2)$$

Where C_0 and C_e are initial and equilibrium concentrations (mg L^{-1}) of uranium ions, respectively. m is the sorbent mass (g) and V is the solution volume (mL). All the reported results are the average of triplicate determinations with the relative errors of less than 5%.

Results and discussion

Characterization

The proximate and ultimate analyses of CPW were carried out based on ASTM-D3172-89 standard method using CHNOS analyzer and the results are tabulated in Table 1.

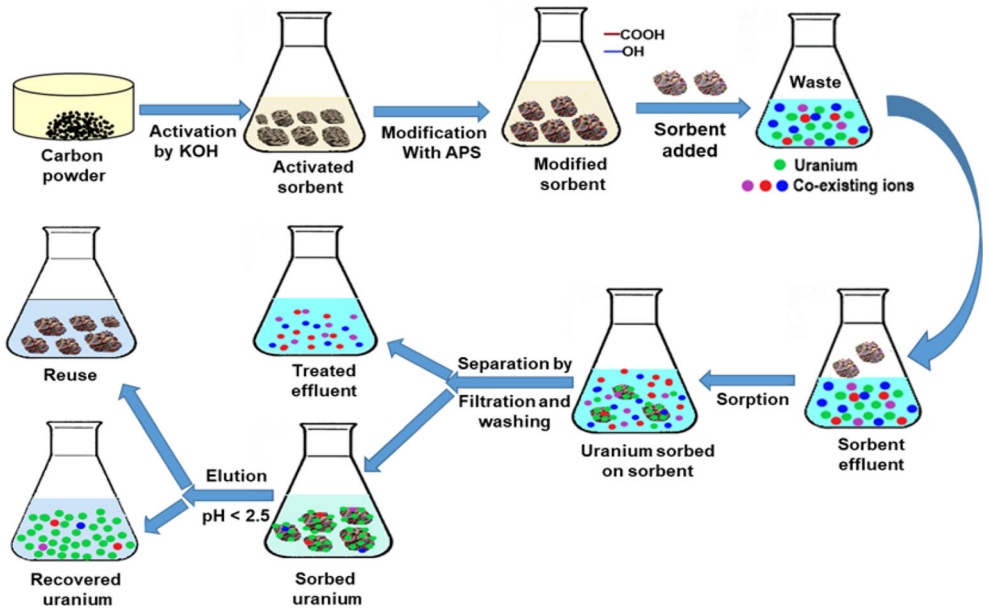

Scheme 1 The process for uranium removal by the proposed method

Table 1 Proximate and ultimate analyses of CPW used for the sorbent preparation

Proximate analysis (wt.%)		Ultimate analysis (wt.%)	
Fixed carbon	92.84	Carbon	95.73
Volatile matter	4.45	Nitrogen	0.25
Ash content	0.52	Hydrogen	1.89
Moisture	2.19	Oxygen (diff.)	1.95
		Sulfur	0.18

Table 2 EDS analysis of A-CPW and A-CPW-COOH

Element	A-CPW		A-CPW-COOH	
	Intensity (c/s)	Conc. (wt %)	Intensity (c/s)	Conc. (wt %)
C	311.45	90.11	857.10	83.75
O	5.81	9.89	33.24	16.25

The microstructure and the morphology of the sorbents were characterized by SEM analysis. The SEM images of the precursor (CPW) and the CPW activated by KOH, $FeCl_3$, and $ZnCl_2$ are shown in Fig. 1. As indicated, the structure of the KOH-activated CPW (Fig. 1b) shows a more porous structure with a large number of micro-sized pores, compared to the other two activators. According to Marsh and Rodriguez-Reinoso (2006), the development of porosity in KOH activation of carbonaceous materials is associated with gasification reaction, which is described in the next sections. The EDS analysis, shown in Table 2, clearly indicates that the oxygen contents on the surfaces of A-CPW and A-CPW-COOH significantly were enhanced after the modification process.

The FT-IR study was carried out to find possible changes in the chemical composition of the sorbents upon oxidation (Wazir et al. 2020). The FT-IR spectra of A-CPW and A-CPW-COOH, shown in Fig. 2a, certainly confirm that oxygen functional groups were generated upon oxidation of A-CPW. This is manifested by new bands for A-CPW-COOH compared to A-CPW at 1704 cm^{-1} attributed to C=O stretching in carbonyl groups and a new strong band centered at 1588 cm^{-1} which can be assigned to carboxyl (COO) groups (Marciniak et al. 2018)

Also, a strong band centered at 1167 cm^{-1} can be related to C–O stretching vibrations of carboxyl and hydroxyl groups. The strong band centered at 3430 cm^{-1} in A-CPW is assigned to –OH stretching vibration and that of A-CPW-COOH can be assigned to the same stretching vibrations of hydroxyl and carboxyl groups. In FT-IR spectra of both A-CPW and A-CPW-COOH, the peaks at 2850–2916 cm^{-1} can be assigned to the symmetric and asymmetric C-H stretching vibrations in aliphatic such as $-CH_3$ or $-CH_2$ (Bandosz et al. 1992). The structural changes of the carbon powder before and after

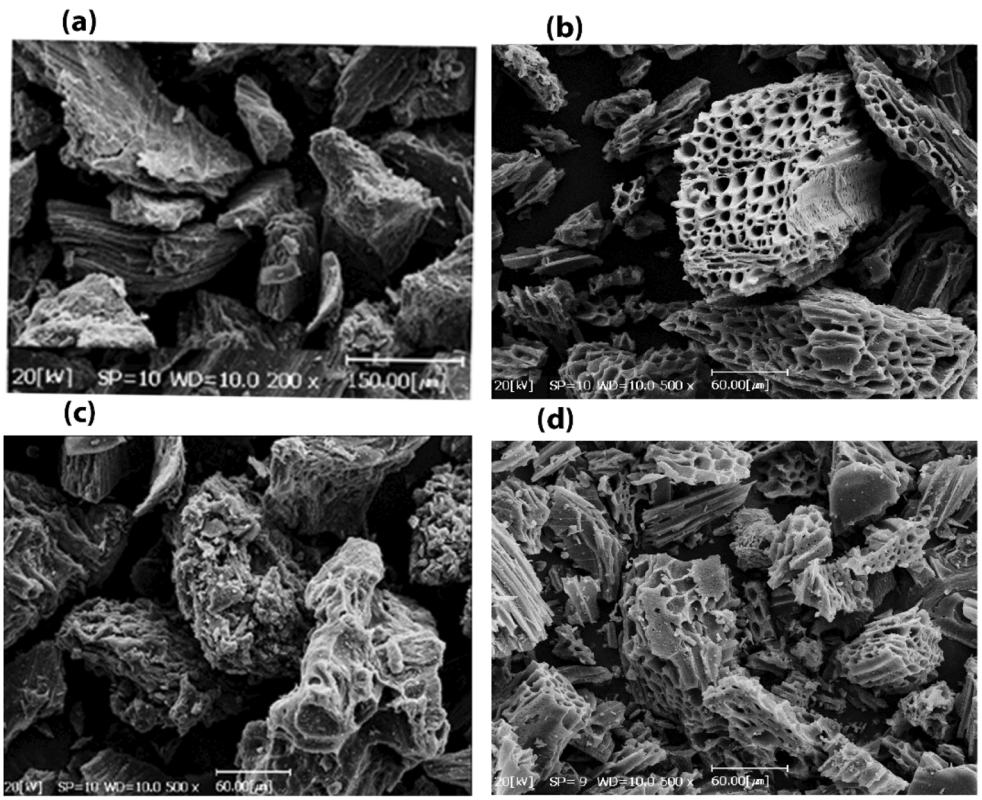

Fig. 1 Scanning electron micrographs (SEM) of **a** the precursor, CPW (**a**), and the CPW activated with KOH (**b**), $FeCl_3$ (**c**), and $ZnCl_2$ (**d**), as activator agents at 725 °C

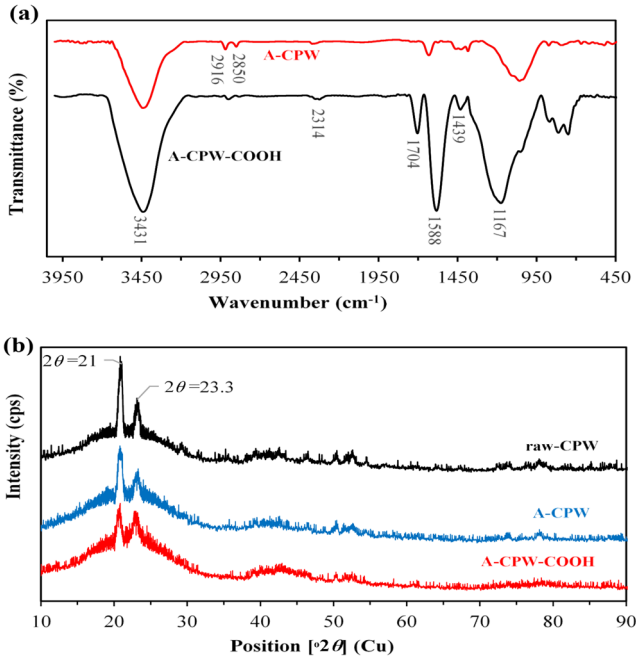

Fig. 2 **a** FT-IR spectra of A-CPW and A-CPW-COOH; **b** the XRD spectra of the sorbents

KOH activation and oxidation were further elucidated by XRD. Figure 2b shows typical XRD patterns of CPW, AC-CPW, and A-CPW-COOH samples. All of the samples displayed a strong broad band centered around 2θ=22° corresponding to the reflection of amorphous carbon framework. In addition, the relatively sharp peaks around 2θ=21.0° and 23.3° can be related to graphite crystallites. The intensity of these peaks which reflect the degree of crystallinity of the carbon decreases from CPW to A-CPW and then further from A-CPW to A-CPW-COOH, indicating that the microcrystallites destroyed in part upon activation by KOH and then oxidation by APS (Chaisit et al. 2020). The weakened diffraction peak intensities also imply that the degree of disorder and porosity have increased.

Activation process

The effect of activation reagents

To amend the adsorption efficiency and selectivity of carbonaceous materials, two main processes of activation and functionalization are required. The activation process can be chemical activation or physical activation. Carbon dioxide and steam are the most common activating agents in physical activation which is performed at temperatures in the range of 700–900 °C (Suárez and Centeno 2020). In the chemical activation process, the most prevalent activating chemicals are phosphoric acid, zinc chloride, sodium or potassium hydroxides, and aluminum chloride. The impregnated material is subsequently carbonized under an inert atmosphere, and then the carbonized material is rinsed to dispel any chemicals and finally a porous structure would be attained (Tsai et al. 2020). Chemical activation is more favorable than physical activation owing to the significant advantages of higher yield, shorter activation time, lower activation temperature, and higher development of porosity (Liew et al. 2018). The carbon powder (CPW) was activated by three chemical activating agents including $ZnCl_2$, KOH, and $FeCl_3$. The effect of activating agents on the porous structure, BET surface area, product yield, total pore volume, and the surface chemistry of the sorbents was investigated. The results in Table 3 indicate that for the sorbent activated by KOH, the yield (86.7%), BET surface area (1380.6 $m^2\ g^{-1}$), pore volume (0.793 $cm^3\ g^{-1}$), and iodine adsorption number (1168 mg g^{-1}) were larger than those of $ZnCl_2$ and $FeCl_3$. Considering that $ZnCl_2$ and $FeCl_3$ are Lewis acids and KOH is a strong base, the experimental results indicate that acidic reagents are not suitable activating agents for CPW as compared to KOH to obtain sorbents with high porosity. It seems that the acidic reagents are more suitable for carbonization of organic materials due to their interaction with functional groups and their catalyzing effect on dehydration and dehydrogenation reactions. In fact, almost all of the applications of these acidic reagents are for carbonization of organic materials (Li et al. 2020a; Yagmur et al. 2020). However, KOH is more suitable for reaction with carbon powder which was used as the raw material in this study to catalyze dehydrogenation as well as oxidation reactions and to enhance porosity of the sorbent. Activation of carbonaceous materials with KOH involves the following gasification reaction:

$$6KOH + 2C \rightarrow 2K + 3H_2 + 2K_2CO_3 \quad (3)$$

$K2CO_3$ further reacts with carbon to form K, K_2O, CO, and CO_2, according to the following reactions (Foo and Hameed 2011):

$$K_2CO_3 + 2C \rightarrow 2K + 3CO \quad (4)$$

$$K_2CO_3 \rightarrow K_2O + CO_2 \quad (5)$$

$$K_2O + C \rightarrow 2K + CO \quad (6)$$

According to Marsh and Rodriguez-Reinoso (2006; Marsh et al. 1984), the liberated potassium metal and possibly other potassium compounds may intercalate into the carbon structure, which results in widening the available pores and generating further porosities. A microporous structure with a new structure is created upon removal of the potassium salts and carbon atoms from the internal volume of the carbon by extensive washing. According to the above reactions, controlling the activation time with KOH at high temperature is highly significant with respect to porosity of the sorbent. The physicochemical properties of the sorbents prepared by different

Table 3 Physicochemical properties of the sorbents prepared with different activating agents

Sorbent	S_{BET} (m^2 g^{-1})	Volume (cm^3 g^{-1})	I_2 number (mg g^{-1})	pH_{pzc}	Product yield (%)	Ash content (%)	Volatile material (%)	Moisture (%)
A-CPW (KOH)	1380.6	0.793	1168	9.7	86.7	2.6	2.2	8.3
A-CPW ($ZnCl_2$)	986.8	0.527	762	6.1	77.8	5.7	7.1	9.2
A-CPW ($FeCl_3$)	722.4	0.387	587	5.2	73.2	8.1	8.7	9.8

activating agents are tabulated in Table 3. According to the above explanations, KOH appears to be a highly efficient chemical activating agent which provides the A-CPW sorbent with the highest porosity and adsorption capacity compared to the other materials studied.

The main physicochemical characteristics of the precursor, KOH-activated CPW (A-CPW), and A-CPW-COOH are given in Table 4. The results indicate that A-CPW-COOH has more acidic surface functional groups than A-CPW. As the result of the modification by oxidation with APS, the pH of the point of zero charge (pH_{pzc}) has decreased from 9.7 for A-CPW to 3.1 for A-CPW-COOH. Decreasing the pH_{pzc} of the modified (A-CPW-COOH) sorbent indicates that the acidic functional groups (-COOH) are well formed on the sorbent surface.

The effect of activation temperature on the surface area

One of the significant advantages of the chemical compared to physical activation is that the process is generally carried out at lower temperature and shorter time. Moreover, carbon sorbents obtained by chemical approach have larger surface area and higher quality than those obtained by physical activation (Om Prakash et al. 2021). The effect of activation temperature on the pore structure of the sorbent was studied in the range of 500–800 °C. The effect of activation temperature on the BET surface area and yield of the product is shown in Fig. 3. As indicated, by increasing the activation temperature from 500 to 725 °C, the BET surface area noticeably increased (Fig. 3a), which can be related to pore formation as a result of evolution of volatile materials from the precursor. At temperatures above 725 °C, extra carbon gasification occurs which undesirably changes the microporous to mesoporous structure. Therefore, the maximum heating temperature during the activation process is really important to the quality of the obtained active carbon.

The effect of activation temperature on the yield of activated carbon was also studied in the temperature range 500–800 °C at constant time of 2 h. The results, shown in Fig. 3b, indicate that the yield of the activated carbon strongly decreases by increasing temperature due to continuous loss of the volatile material. Potassium hydroxide as a strong base may catalyze the oxidation reactions at high temperatures.

Optimization of uranium removal and recovery

The optimization process of the proposed method was carried out through the one-at-the-time method and experimental design using response surface design method (RSM). The effects of different parameters such as contact time, pH of the solution, initial concentration of uranium, and temperature on the uranium sorption amount on the sorbent and modified sorbent were explored. The obtained results by RSM and one-at-the-time method were acceptably in agreement.

The effect of temperature on U(VI) removal

Temperature as a dominant factor in the removal processes is influenced by the nature of the adsorption on the sorbent which can be exothermic or endothermic. The effect of temperature on the sorption capacity of U(VI) ions was studied in the range of 10–50 °C. The adsorption amount of U(VI) increased from 10 to 35 °C, and then decreased from temperatures higher than 35 °C. The results in Fig. 4a confirm the endothermic nature of the dehydration process of UO_2^{2+} ions before their sorption on the solid surface and also the

Table 4 Characteristics and amounts of oxygen functional groups in the sorbents

Sorbents	S_{BET} (m^2 g^{-1})	Volume (cm^3 g^{-1})	I_2 number (mg g^{-1})	pH_{pzc}	Amounts of oxygen-containing functional groups (mmol g^{-1})				
					Carboxylic	Lactonic	Phenolic	Acidic	Basic
CPW	46.4	0.034	27.6	-	-	-	-	-	-
A-CPW	1380.6	0.793	1168	9.7	0.031	0.278	0.625	0.272	2.814
A-CPW-COOH	978.9	0.533	762	3.1	3.482	0.672	1.946	4.653	0.725

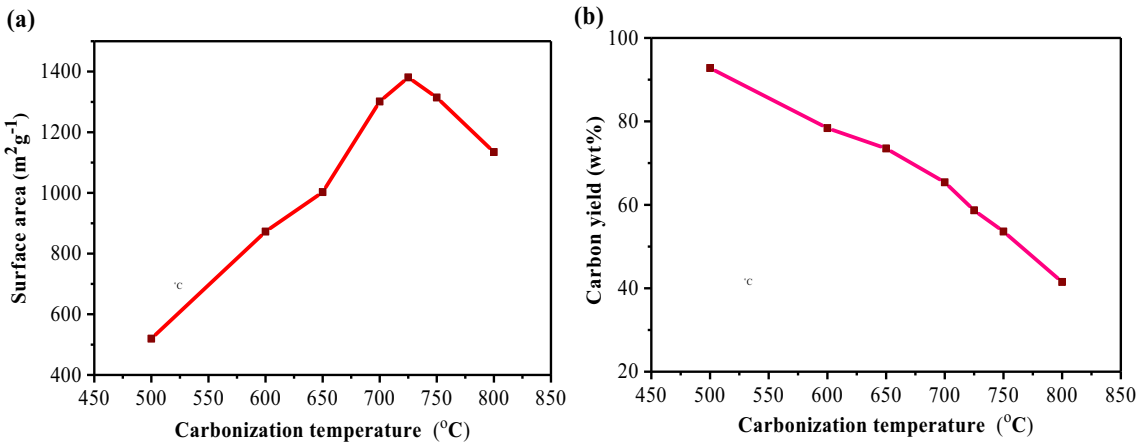

Fig. 3 The effect of activation temperature on the **a** surface area, and **b** carbon yield (%) of the A-CPW

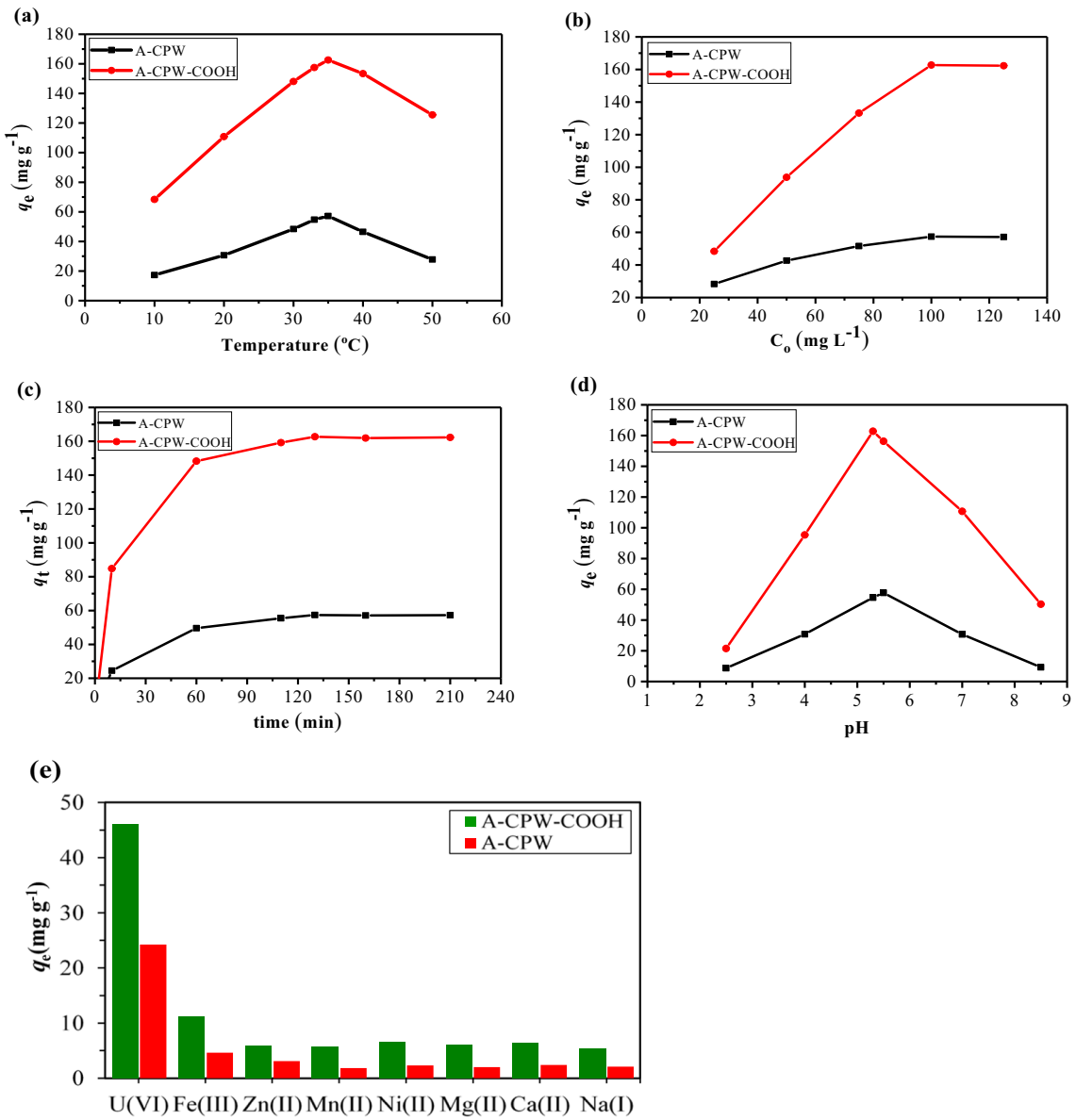

Fig. 4 The effect of **a** temperature, **b** initial uranium concentration, **c** contact time, **d** pH, and **e** interfering ions on U(VI) adsorption interfering

increment of UO_2^{2+} ion mobility. For the temperatures above 35 °C, the kinetic energy and the mobility of the ions extremely increase and prevent ion adsorption on the sorbent surface. Also higher temperatures cause less stability of the interactions between UO_2^{2+} ions and active sites on the sorbent surface. Therefore, the optimum temperature of 35 °C was chosen for the rest of studies.

The effect of the initial uranium concentration

In order to investigate the effect of initial uranium concentration on the sorption amount, various concentrations of U (VI) in the range of 25, 50, 75, 100, and 125 mg L^{-1} were studied at pH of 5.5 and 5.3 for A-CPW and A-CPW-COOH, respectively, using 50 mg of the sorbent at 35 °C for 130 min. The results in Fig. 4b indicate that the adsorption amount increased from 25 to 100 mg L^{-1} and then decreased. By increasing the initial uranium concentration from 10 to 100 mg L^{-1}, the enhancement in adsorption of UO_2^{2+} ions occurs which may be due to the enhancement of a larger driving force compared to the mass transfer resistance between the sorbent and liquid phases. Hence, the interaction of analyte-sorbent and also the occupation of the sorbent active sites would be augmented by the uranium ions (Abutaleb et al. 2020; Qu et al. 2021). However, for the concentrations above 100 mg L^{-1}, the repulsive force of uranium ions and the saturation of the sorbent

Table 5 Experimental matrix of five-level four-factor CCD for removal of uranium from effluents by A-CPW-COOH

Experiment No.	Factors				q_e (mg g^{-1})	
	pH	Time (min)	Temperature (°C)	Initial uranium conc. (mg L^{-1})	Experimental values	Predicted values
1	4.0	60	20	100	120.2	120.56
2	5.5	110	30	75	147.1	147.66
3	5.5	110	50	75	135.2	133.87
4	2.5	110	30	75	107.3	107.10
5	7.0	60	40	100	136.2	137.82
6	5.5	110	30	75	149.5	147.66
7	4.0	160	20	100	143.3	145.06
8	7.0	60	20	50	84.2	83.95
9	5.5	110	10	75	117.0	117.97
10	5.5	110	30	75	149.3	147.66
11	5.5	110	30	75	146.0	147.66
12	7.0	160	20	50	94.5	95.25
13	7.0	160	40	50	92.2	92.28
14	4.0	60	40	50	82.5	81.93
15	7.0	60	40	50	94.7	92.88
16	4.0	60	20	50	68.3	66.61
17	4.0	160	40	100	152.8	152.03
18	7.0	160	20	100	137.1	136.65
19	5.5	10	30	75	101.5	102.97
20	7.0	60	20	100	126.2	125.35
21	5.5	210	30	75	128.7	126.87
22	4.0	60	40	100	138.8	139.43
23	5.5	110	30	25	48.1	49.52
24	5.5	110	30	125	150.2	148.42
25	5.5	110	30	75	147.0	147.66
26	8.5	110	30	75	109.8	109.63
27	4.0	160	20	50	92.3	91.11
28	5.5	110	30	75	149.0	147.66
29	4.0	160	40	50	92.3	94.53
30	7.0	160	40	100	135.6	137.22
31	5.5	110	30	75	145.7	147.66

Table 6 Regression coefficients, *t*-values, and *p*-values of the model estimated by Minitab software for separation of uranium, b_0 = constant, x_1 = pH, x_2 = temperature (°C), x_3 = time (min), x_4 = initial uranium concentration (mg L^{-1})

Term	Coefficient	SE (Coeff.)	*t*-value	*p*-value
b_0	147.657	0.672	219.76	0.000
x_1	0.633	0.363	1.75	0.096
x_2	3.975	0.363	10.95	0.000
x_3	5.975	0.363	16.47	0.000
x_4	24.725	0.363	68.14	0.000
x_1^2	−9.823	0.332	−29.55	0.000
x_2^2	−5.435	0.332	−16.35	0.000
x_2^3	−8.185	0.332	−24.62	0.000
x_2^4	−12.173	0.332	−36.62	0.000
$x_1 \times x_2$	−1.600	0.444	−3.60	0.002
$x_1 \times x_3$	−3.300	0.444	−7.43	0.000
$x_1 \times x_4$	−3.138	0.444	−7.06	0.000
$x_2 \times x_3$	−2.975	0.444	−6.69	0.000
$x_2 \times x_4$	0.888	0.444	2.00	0.063
$x_3 \times x_4$	0.363	0.444	0.82	0.427

active sites by uranium ions reduce the adsorption amount. By increasing initial concentration of U(VI), the removal efficiency of UO_2^{2+} ions would decrease. The maximum amount of adsorption was obtained at the concentration of 100 mg L^{-1}.

The effect of contact time

The equilibrium between the adsorbate and adsorbent in removal processes determines the removal efficiency. Proper contact time is required to achieve maximum removal (%). Therefore, the contact time was studied in the range of 10–210 min by stirring 50 mg of A-CPW and A-CPW-COOH with 100 mL of 100 mg L^{-1} uranium at 35 °C and the results are presented in Fig. 4c. As the results show, the adsorption of U(VI) on the sorbent surface rapidly increased from 10 to 60 min and after that a slow rise was observed and then became constant after 130 min. Apparently, the U(VI) adsorption attained the equilibrium state after 130 min, which was used as the optimum contact (stirring) time.

The effect of solution pH

The pH of the solution has an indicative role in adsorption of UO_2^{2+} ions on the sorbents through controlling the surface functional group charge and binding sites of the adsorbent. The solution pH in the range of 2.5–8.5 was studied using optimum values of temperature (35 °C), U(VI) concentration (100 mg L^{-1}), and stirring time (130 min). According to the obtained results in Fig. 4d, the adsorption of U(VI) increases from 2.5 to 5.5, and then decreases for the pH > 5.5. At pH values below 5.5, free species of UO_2^{2+} are the dominant in the solution. When the pH of the solution increases above 5.5, the hydrolysis of UO_2^{2+} ions to form $UO_2(OH)_2^0$, $UO_2(OH)^+$, $(UO_2)_2(OH)_2^{2+}$, and $(UO_2)_3(OH)_5^{3+}$ takes place. However, at pH > 7.0, the surface charge of sorbents is more negative, but the species such as $UO_2(OH)_3^-$, $(UO_2)_3(OH)_7^-$, $UO_2(CO_3)_2^{2-}$, and $UO_2(CO_3)_3^{4-}$ are formed in the solution, which reduces the amounts of UO_2^{2+} adsorbed on sorbents (Basile et al. 2017; Zhong et al. 2021). Therefore, the optimum pH of 5.5 was chosen for further studies.

Experimental design and analysis

The experimental and CCD predicted values of q_e, obtained as response for 31 experimental runs which were performed in randomized order, are presented in Table 5. The experimental sorption capacity, q_e (mg g^{-1}), obtained from each point of the CCD design was analyzed by statistical regression analysis and analysis of variance (ANOVA) using the Minitab software. The regression coefficients for all the parameters are given in Table 6. At 95% confidence level, the *p*-values of <0.05 indicate that the coefficient is significant and can be included in the model. The smaller the *p*-value, the more significant is the related coefficient. However, as can be seen in Table 6, most of the *p*-values are 0, which does not show the

Table 7 Analysis of variance (ANOVA) for fitting the experimental data for sorption by A-CPW-COOH

Sources	Degree of freedom	Adjusted sum of squares	Adjusted mean squares	F value	*p* value
Regression	14	24,091.2	1720.8	544.54	0.00
Linear	4	15,917.5	3979.4	1259.26	0.00
Square	4	7644.7	1911.2	604.79	0.00
Interaction	6	529.0	88.2	27.9	0.00
Residual error	16	50.6	3.2	-	
Lack-of-fit	10	35.3	3.5	1.39	0.36
Pure error	6	15.2	2.5	-	-
Total	30	24,141.8	-	-	-

influential extent of the significant factors. In this regard, the *t*-values are more informative because the larger the *t*-value, the more significant is the coefficient.

The statistical analysis (ANOVA) results including the estimated regression coefficients and *p*-values are shown in Table 7. The lack-of-fit term is not significant (*p*-value = 0.36 is much higher than the 0.05). This term can also be evaluated using the *F*-test. The calculated *F*-value for the lack-of-fit (1.39), which is significantly lower than the critical value (F_{crit} = 4.06), indicates that the model fitted well with the data and also the applied model has successfully created an ideal prediction for the process. Using the coefficients given in Table 6, the model predicted for removal of uranium by A-CPW-COOH is presented in Eq. 7:

$$\begin{aligned} q_e = {} & -372.01 + 62.760\ \mathrm{pH} + 4.633\ \mathrm{temp} + 1.239\ \mathrm{time} \\ & + 4.232\ \mathrm{conc} - 4.366\ (\mathrm{pH})^2 - 0.054\ (\mathrm{temp})^2 - 0.003 \\ & (\mathrm{time})^2 - 0.019\ (\mathrm{conc})^2 - 0.107\ \mathrm{pH} \\ & \times \mathrm{temp} - 0.044\ \mathrm{pH} \times \mathrm{time} - 0.084\ \mathrm{pH} \\ & \times \mathrm{conc} - 0.006\ \mathrm{temp} \times \mathrm{time} + 0.004\ \mathrm{temp} \times \mathrm{conc} \\ & + 0.0003\ \mathrm{time} \times \mathrm{conc} \end{aligned} \quad (7)$$

The plot of the experimental data versus predicted data had the linear regression coefficient (R^2) of 0.9978 (*SE*= 1.78), which confirms a good agreement between predicted and experimental responses. The adjusted R^2 of the process was 99.62% that reveals the ability of the developed model to predict the adsorption amount of uranium ions. Moreover, the predicted results by RSM are shown in Fig. 5. The predicted optimum results by RSM appropriately correspond with the one-at-a-time experimental data. The optimum conditions to achieve the q_e of 162.47 mg g^{-1} (*SE*= 0.725) were predicted at the temperature of 33.30 °C, pH of 5.31, time of 130.19 min, and initial uranium concentration of 100.76 mg L^{-1}.

Adsorption isotherm studies

The equilibrium attainment between the sorbent and the analyte is definitely important in any adsorption process, which makes a logical relationship between the sorption extent and the analyte equilibrium concentration (Hassani et al. 2017). This relationship at constant temperature is defined as adsorption isotherm which clarifies the features and the nature of the adsorption process. Hence, various models can be applied to depict the details of the process. Herein, in order to scrutinize the sorption performance and the interaction between UO_2^{2+} ions and the sorbent and to evaluate the sorption capacity of the A-CPW-COOH, the experimental equilibrium data were analyzed according to Langmuir and Freundlich (Ganguly et al. 2020; Nnadozie and Ajibade 2020).

The Langmuir isotherm theory is used to describe the monolayer adsorption on the homogeneous surface without any interaction between the adsorbed molecules. This model assumes that the adsorption occurs uniformly on the active sites within the sorbent and only once an adsorbate can successfully capture a site. The Langmuir isotherm can be represented by Eq. 8 (Côrtes et al. 2019; Yildirim et al. 2020).

$$q_e = \frac{q_m K_L C_e}{1 + K_L C_e} \quad (8)$$

where q_e is the amount of uranium ions adsorbed at equilibrium (mg g^{-1}), C_e is the equilibrium concentration of

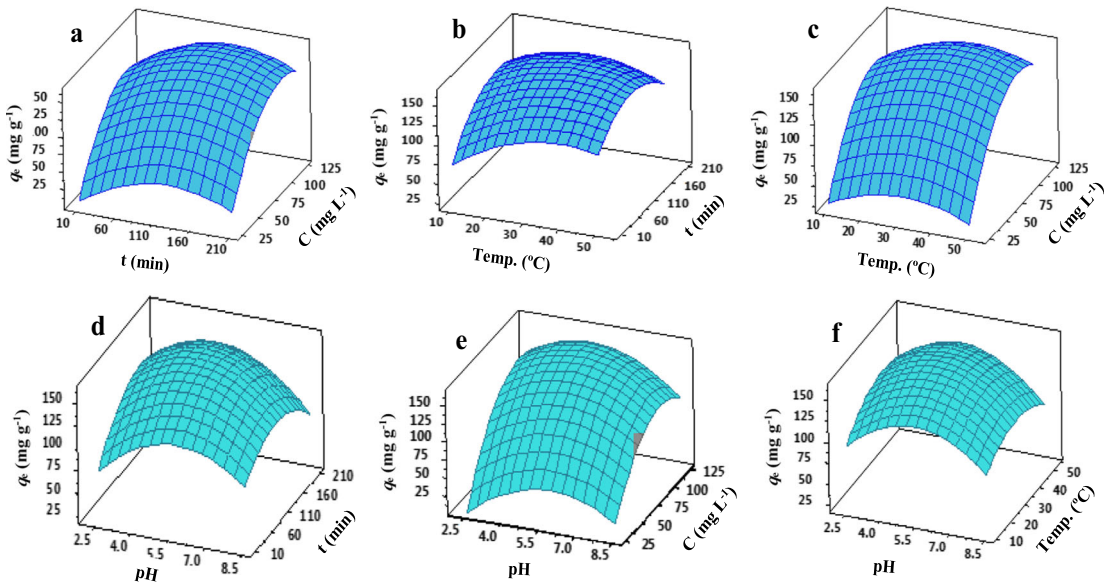

Fig. 5 Response surface plots of parameters for uranium sorption by A-CPW-COOH

Table 8 Isotherm parameters for U(VI) adsorption on A-CPW-COOH at T= 308 K and C_0= 100 mg L^{-1}

Langmuir		Freundlich	
q_m (mg g^{-1})	192.31	1/n	0.5835
K_L	0.3421	K_F	54.806
R^2	0.9994	R^2	0.9974
R^2_{adj}	0.9987	R^2_{adj}	0.9948
RSS (*)	2.6991e^{-5}	RSS	0.0027
RMSE (**)	0.0124	RMSE	0.1127

*Residual sum of squares

**Root mean square error

uranium in solution (mg L^{-1}), q_m (mg g^{-1}) is the maximum sorption capacity, and K_L (L mg^{-1}) is the Langmuir constant related to the energy and the rate of sorption. The values of q_m and K_L were calculated using Eq. 8.

The Freundlich isotherm theory considers the sorbent surface as the heterogeneous and assumes several kinds of sites on the sorbent with difference adsorption energies. The nonlinear equation of the Freundlich isotherm is as follows:

$$q_e = K_F C_e^{\frac{1}{n}} \tag{9}$$

where K_F ((mg g^{-1}) (mg L^{-1})$^{-1/n}$) and 1/n are the Freundlich constants, which related to the capacity and intensity of adsorption, respectively. The amount of $(\frac{1}{n})$ < 1 indicates the favorability of UO_2^{2+} ion adsorption on the sorbents. The isotherm models of Langmuir and Freundlich were used to estimate the equilibrium parameters. The results of Table 8 indicate that the Langmuir model due to its higher values of R^2 =0.9994 and R^2_{adj} = 0.9987 and lower values of RMSE= 0.0124 is more suitable for uranyl adsorption on A-CPW-COOH than the Freundlich model (Fig. 6). Moreover, the monolayer sorption takes place in homogeneous adsorption sites on the sorbents and the interaction is weak and can be ignored. The values of n (n >1) in Table 8 represent that the sorption of UO_2^{2+} ions on the A-CPW-COOH is extremely favorable. The value of maximum capacity (q_m) obtained from the Langmuir model at 308 K for A-CPW-COOH was 192.31 mg g^{-1}, which indicates that adsorption capacity of A-CPW-COOH is considerably increased.

Kinetics studies

Fast removal of the target analyte in a removal process not only ascertains high efficiency of the sorbent but also shortens the time to accomplish the process. The kinetics of UO_2^{2+} adsorption process on A-CPW-COOH was considered using the pseudo-first-order (Eq. 10) and second-order (Eq. 11) kinetic equations as follows (Côrtes et al. 2019):

$$q_t = q_e(1-\exp(-k_1 t)) \tag{10}$$

$$q_t = \frac{t}{(1/k_2 q_e^2) + (t/q_e)} \tag{11}$$

In which k_1 (min^{-1}) and k_2 (g mg^{-1} min^{-1}) are the pseudo-first-order and pseudo-second-order rate constants, respectively. q_e and q_t are the adsorption amounts of uranyl ion (mg g^{-1}) at equilibrium and time "t," respectively. In order to better understand the adsorption process, kinetic curves were fitted with the pseudo-first-order and pseudo-second-order models (Fig. 7). The values of k_1, q_e, and k_2 were estimated from the slopes and the intercepts of the plots shown in the Fig. 7 using Eqs. 10 and 11. The kinetic parameters are presented in Table 9. The favorable model was selected by the evaluation of R^2, R^2_{adj}, and RMSE. According to the obtained results, the higher values of R^2 and R^2_{adj} were calculated using the pseudo-second-order model. Therefore, the pseudo-second-order model with correlation coefficient of R^2 =0.9998, R^2_{adj} = 0.9997, and RMSE=0.0058 is more desirable than the pseudo-first-order model with R^2 =0.9948, R^2_{adj} = 0.9930, and RMSE = 0.1469 to predict the UO_2^{2+} ion adsorption on

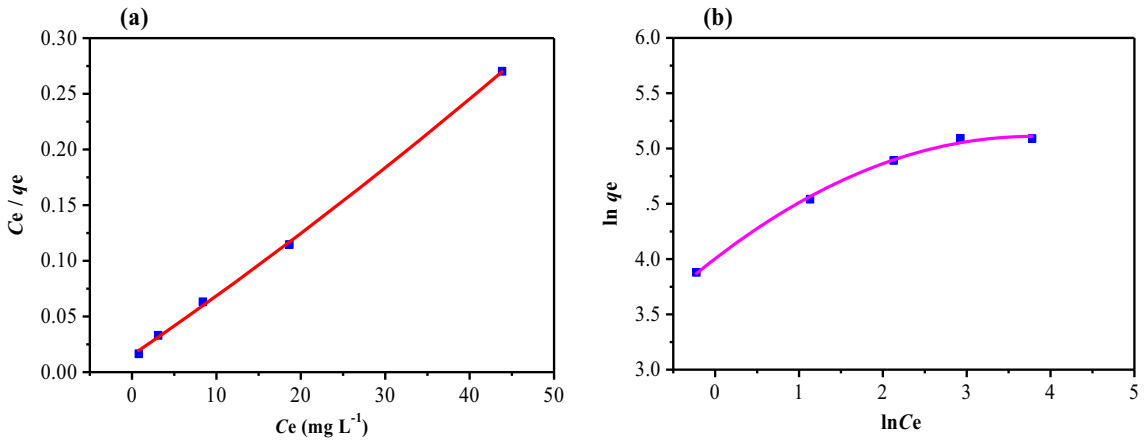

Fig. 6 The adsorption isotherms for U(VI) adsorption on A-CPW-COOH including **a** Langmuir and **b** Freundlich

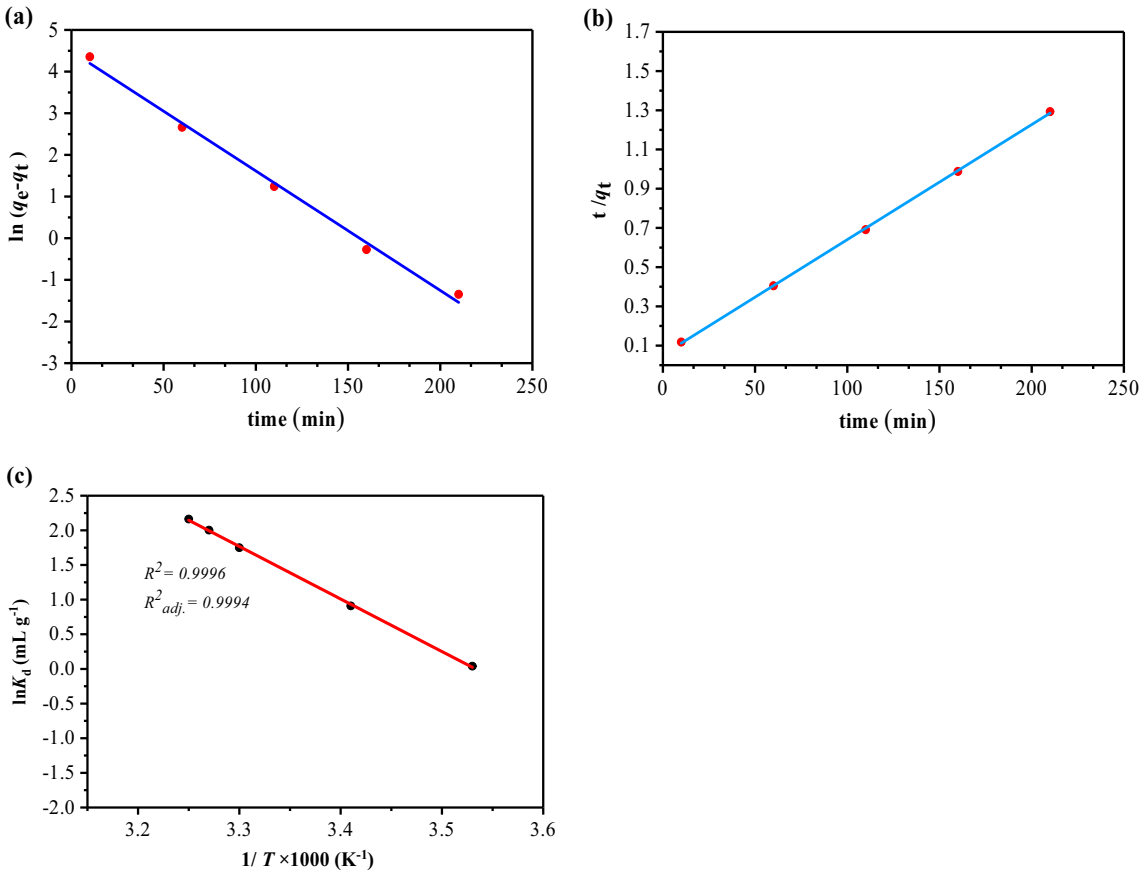

Fig. 7 **a** Pseudo-first-order kinetic model, **b** pseudo-second-order kinetic model, and **c** the thermodynamics of U(VI) adsorption on A-CPW-COOH

A-CPW-COOH. Also, the calculated values of the equilibrium adsorption capacities of A-CPW-COOH by second-order model for $q_{e,\ cal.}$ (169.49 mg g^{-1}) are close to the experimental adsorption capacity, $q_{e,\ exp.}$ (162.66 mg g^{-1}). Therefore, this model was able to predict very accurately the experimental values of adsorption capacity ($q_{e(exp)}$).

Table 9 Kinetic parameters for the adsorption of U(VI) on A-CPW-COOH

Pseudo-first-order kinetics		Pseudo-second-order kinetics	
$q_{e\ (exp)}$ (mg g^{-1})	162.66	$q_{e\ (exp)}$ (mg g^{-1})	162.66
$q_{e\ (cal)}$ (mg g^{-1})	88.52	$q_{e\ (cal)}$ (mg g^{-1})	169.49
k_1 (min^{-1})	2.87×10^{-2}	k_2 (g mg^{-1} min^{-1})	6.51×10^{-4}
R^2	0.9948	R^2	0.9998
R^2_{adj}	0.9930	R^2_{adj}	0.9997
RSS (*)	0.1079	RSS	$1.6896e^{-4}$
RMSE (**)	0.1469	RMSE	0.0058

*Residual sum of squares

**Root mean square error

Thermodynamic studies

To assess the thermodynamic behavior of the U(VI) ions onto the sorbent, the thermodynamic values including enthalpy change ($\Delta H°$) and entropy change ($\Delta S°$) and Gibbs free energy ($\Delta G°$) were calculated from the following equations:

$$K_d = \frac{C_0 - C_e}{C_e} \times \frac{V}{m} \quad (12)$$

$$\Delta G = -RT \ln(K_d) \quad (13)$$

$$\ln K_d = \frac{\Delta S}{R} - \frac{\Delta H}{RT} \quad (14)$$

$$\Delta G = \Delta H - T\Delta S \quad (15)$$

Table 10 Thermodynamic parameters for adsorption of U(VI) onto A-CPW-COOH

Temperature (K)	$\Delta G°$ (kJ mol^{-1})	$\Delta H°$ (kJ mol^{-1})	$\Delta S°$ (kJ mol^{-1} K^{-1})
293	−65.20		-
303	− 67.42	-	-
308	− 68.54	63.060	0.223

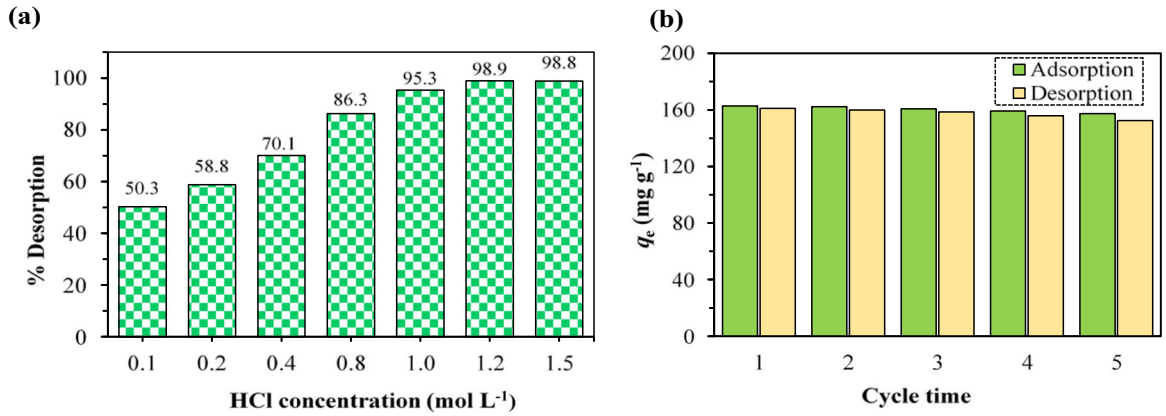

Fig. 8 **a** The effect of HCl solution concentration on desorption (%) of U(VI), **b** the sequential sorption/desorption cycles of U(VI).

Where K_d is the distribution coefficient (mL g^{-1}), ΔS is the entropy change (J mol^{-1} K^{-1}), ΔH is the enthalpy change (kJ mol^{-1}), T is the absolute temperature (K), and R is the gas constant (8.314 kJ mol^{-1}). The value of K_d was calculated using Eq. 12. The value of ΔS was estimated from the intercept of the plot of ln(K_d) versus 1/T (Fig. 7c) by Eq. 14. The values of ΔH and ΔG were calculated by Eqs. 14 and 15, respectively. The calculated values of thermodynamic parameters are presented in Table 10. The negative values of ΔG demonstrate spontaneous nature and feasibility of the process of uranium sorption on the sorbents. The results of Table 10 show that the ΔG value at 308 K for A-CPW-COOH increases, indicating the role of functional groups on improving U(VI) adsorption onto A-CPW-COOH. The positive value of enthalpy change (ΔH) demonstrates that the sorption process of UO_2^{2+} ions on A-CPW-COOH is endothermic, indicating that the sorption process is more favorable at higher temperatures. This behavior can be explained by considering the hydration layer of UO_2^{2+} ions that must be removed before it can be adsorbed on the sorbent surface. This dehydration process requires energy and it is more favorable at higher temperatures. The positive value of entropy change (ΔS) indicates some structural changes in adsorbed ions and sorbent during the sorption process, which leads to an increase in the disorder of the solid–liquid system.

Reusability of the sorbent

The reusability and regeneration of the used sorbent are indicative factors in any removal process. To this aim, HCl solution was used as a desorbing agent to recover the sorbent and elute uranium from the sorbent structure. The concentration of HCl solutions in the range from 0.1 to 1.5 mol L^{-1} was investigated; and according to the obtained results in Fig. 8a, the concentration of 1.2 mol L^{-1} of HCl was chosen for regeneration of the sorbent. After five sequential sorption/desorption cycles, the uranium uptake capability decreased from 162.8 in the first cycle to 157.4 mg g^{-1} in the fifth cycle Fig. 8b. The results showed that U(VI) loaded onto A-CPW-COOH could be effectively regenerated by 1.2 mol L^{-1} HCl and reused with only slight influence on its U(VI) sorption capability after 5 cycles.

Removal mechanism

The remarkable effect of pH on the sorption capacity indicates that the sorption of UO_2^{2+} onto A-CPW-COOH is affected by the surface functional group status due to their protonation or deprotonation behavior (Cheng et al. 2019; Zhang et al. 2020a). At low pH values (pH < pH_{PZC}), the carboxyl and hydroxyl groups on A-CPW-COOH will be highly protonated

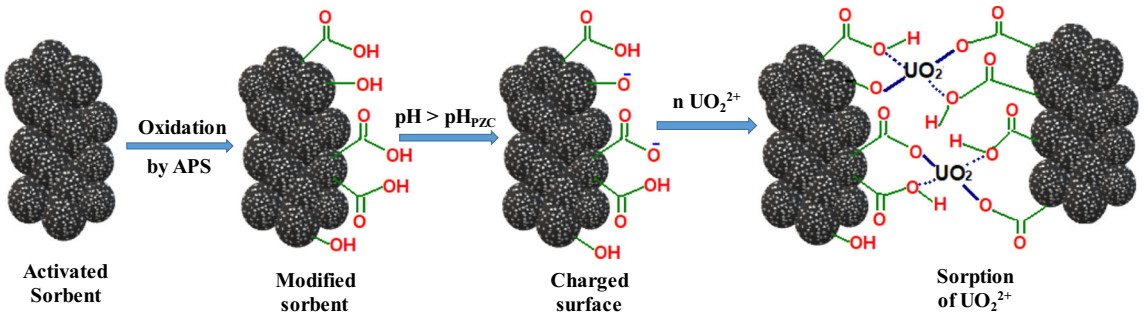

Scheme 2 Schematic representation of the modification process of A-CPW and interaction of A-CPW-COOH with uranyl ions

Table 11 Comparison of the selectivity of the sorbents A-CPW and A-CPW-COOH towards different metal ions

Metal ion	K_d (mL g^{-1})		S		S_r (relative selectivity coefficient)
	A-CPW	A-CPW-COOH	A-CPW	A-CPW-COOH	
U(VI)	1891.05	24315.79	-	-	-
Fe(III)	202.64	577.32	9.33	42.12	4.51
Zn(II)	132.20	267.57	14.30	90.88	6.35
Mn(II)	74.69	257.34	25.32	94.49	3.73
Ni(II)	96.44	304.15	19.61	79.95	4.08
Mg(II)	83.33	277.90	22.69	87.50	3.86
Ca(II)	100.84	298.85	18.75	81.36	4.34
Na(I)	87.68	242.15	21.57	100.42	4.66

m = 0.05 g, V = 100 mL, C_0 = 25 mg L^{-1}, T = 308 K, pH = 5.3

which leads to decrement of carboxyl groups nucleophilicity towards U(VI) and limiting the U(VI) sorption onto the sorbent. With increasing pH (pH > pH_{PZC}) (for A-CPW-COOH, pH_{PZC} = 3.1) (Table 4), the protonation degree of the carboxyl groups will be reduced and it is easier to separate the hydroxyl protons in carboxyl groups. Therefore, the lone-pair electron on the negative charged oxygen of COO^- group interacts with the empty orbits of U(VI), and accordingly favoring the formation of the complex as shown in Scheme 2.

Adsorption selectivity

To evaluate the selectivity of A-CPW and A-CPW-COOH in uranium ion removal, a simulated nuclear fuel effluent containing some metal ions including Mg^{2+}, Na^{+}, Zn^{2+}, Mn^{2+}, Ni^{2+}, and Fe^{3+} was prepared and treated with A-CPW and A-CPW-COOH at the optimal conditions. The obtained results, shown in Fig. 4e, revealed that A-CPW-COOH has better selectivity and high adsorption capacity toward U(VI) than the other existing ions. The selectivity coefficient ($S_{UO_2^{2+}/M^{n+}}$) for uranyl ions relative to competing ions is estimated by the following equation (Elsayed et al. 2021):

$$S_{\left(UO_2^{2+},/,M^{n+}\right)} = \frac{K_d^{UO_2^{2+}}}{K_d^{M^{n+}}} \quad (16)$$

where $K_d^{UO_2^{2+}}$ and $K_d^{M^{n+}}$ are distribution coefficients of uranyl ions and the interference ions, respectively. The values of $S_{UO_2^{2+}/M^{n+}}$ in Table 11 show higher selectivity of A-CPW-COOH towards A-CPW which corroborates the desirable performance of A-CPW-COOH in interaction of carboxylic acid functional groups with uranium ion. Moreover, Table 9 acceptably confirms better selectivity coefficients of A-CPW-COOH for U(VI) ions over a range of competing metal ions.

Conclusions

In the present study, carbon powder waste from zirconium carbide industry was used as the raw material for preparation of activated modified carbon adsorbent which was used for uranium removal from waste radioactive effluents of the nuclear industry. The activation and modification of the CPW improved the adsorption performance and efficiency of the obtained sorbent in uranium ion removal. Among several activating agents ($ZnCl_2$, KOH, and $FeCl_3$) that were examined for activation of CPW, KOH provided the highest BET surface area and porosity. The sorbent obtained from KOH was modified by the simple oxidation method using APS which enhances the uranium removal efficiency through carboxylic acid functional groups. The kinetic studies UO_2^{2+} ion sorption can be described more favorably by the pseudo-second-order kinetic model. The Langmuir model fitted the sorption isotherms better than the Freundlich and Timken models. The maximum U(VI) sorption capacity of A-CPW-COOH obtained by the Langmuir model was estimated to be 192.31 mg g^{-1}, which confirms the sorption capacity of A-CPW-COOH. The enthalpy values ($\Delta H_{A\text{-}CPW\text{-}COOH}$ = 63.06 (kJ mol^{-1})) demonstrate that the sorption of U(VI) on A-CPW-COOH was endothermic. The entropies ($\Delta S_{A\text{-}CPW\text{-}COOH}$ = 0.223 (kJ mol^{-1} K^{-1})) and Gibbs free energies ($\Delta G_{A\text{-}CPW\text{-}COOH}$ = −68.54 (kJ mol^{-1})) at T= 308 K all indicate that the uranium uptake by the sorbents was spontaneous. The process can be easily scaled up industrially which intensifiers the advantage of the proposed process.

Acknowledgements The authors appreciate the supports provided by the Graduate Office of the University of Shahrekord.

Author contributions Majid Mohammad Nezhad: investigation, writing-original draft, conceptualization and methodology. Abolfazl Semnani and Nahid Tavakkoli: conceptualization, editing, and supervision. Mahboube Shirani: data curation and software, writing of original draft.

Availability of data and materials The datasets generated and/or analyzed during the current study are not publicly available due to the policies of the nuclear fuel factory in Isfahan but are available from the corresponding author on reasonable request.

Declarations

Ethics approval and consent to participate Not applicable.

Consent for publication Not applicable.

Competing interests The authors declare no competing interests.

References

Abutaleb A, Tayeb AM, Mahmoud MA, Daher AM, Desouky OA, Bakather OY, Farouq R (2020) Removal and recovery of U(VI) from aqueous effluents by flax fiber: adsorption, desorption and batch adsorber proposal. J Adv Res 22:153–162. https://doi.org/10.1016/j.jare.2019.10.011

Bandosz TJ, Jagiello J, Schwarz JA (1992) Comparison of methods to assess surface acidic groups on activated carbons. Anal Chem 64: 891–895. https://doi.org/10.1021/ac00032a012

Basile M, Unruh DK, Streicher L, Forbes TZ (2017) Spectral analysis of the uranyl squarate and croconate system: evaluating differences between the solution and solid-state phases. Cryst Growth Des 17: 5330–5341. https://doi.org/10.1021/acs.cgd.7b00838

Boehm HP (2002) Surface oxides on carbon and their analysis: a critical assessment. Carbon 40:145–149. https://doi.org/10.1016/S0008-6223(01)00165-8

Brunauer S, Emmett PH, Teller E (1938) Adsorption of gases in multimolecular layers. J Am Chem Soc 60:309–319. https://doi.org/10.1021/ja01269a023

Chaisit S, Chanlek N, Khajonrit J, Sichumsaeng T, Maensiri S (2020) Preparation, characterization, and electrochemical properties of KOH-activated carbon from cassava root Materials Research Express 7:105605. https://doi.org/10.1088/2053-1591/abbf84

Cheng Y, He P, Dong F, Nie X, Ding C, Wang S, Zhang Y, Liu H, Zhou S (2019) Polyamine and amidoxime groups modified bifunctional polyacrylonitrile-based ion exchange fibers for highly efficient extraction of U(VI) from real uranium mine water. Chem Eng J 367: 198–207. https://doi.org/10.1016/j.cej.2019.02.149

Chung Y, Yun Y-M, Kim Y-J, Hwang YS, Kang S (2018) Preparation of alumina-zirconia (Al-Zr) ceramic nanofiltration (NF) membrane for the removal of uranium in aquatic system. Water Supply 19:789–795. https://doi.org/10.2166/ws.2018.123

Côrtes LN et al. (2019) Biochars from animal wastes as alternative materials to treat colored effluents containing basic red 9 Journal of Environmental Chemical Engineering 7:103446. https://doi.org/10.1016/j.jece.2019.103446

Deng H, Z-j L, Wang L, L-y Y, J-h L, Z-y C, Z-f C, W-q S (2019) Nanolayered Ti3C2 and SrTiO3 composites for photocatalytic reduction and removal of uranium(VI). ACS Appl Nano Mater 2: 2283–2294. https://doi.org/10.1021/acsanm.9b00205

Duan J, Ji H, Xu T, Pan F, Liu X, Liu W, Zhao D (2021) Simultaneous adsorption of uranium(VI) and 2-chlorophenol by activated carbon fiber supported/modified titanate nanotubes (TNTs/ACF): effectiveness and synergistic effects. Chem Eng J 406:126752. https://doi.org/10.1016/j.cej.2020.126752

Elsayed NH, Alatawi RAS, Monier M (2021) Amidoxime modified chitosan based ion-imprinted polymer for selective removal of uranyl ions. Carbohydr Polym 256:117509. https://doi.org/10.1016/j.carbpol.2020.117509

Foo KY, Hameed BH (2011) Utilization of rice husks as a feedstock for preparation of activated carbon by microwave induced KOH and K2CO3 activation Bioresource Technology 102:9814-9817. https://doi.org/10.1016/j.biortech.2011.07.102

Ganguly P, Sarkhel R, Das P (2020) Synthesis of pyrolyzed biochar and its application for dye removal: batch, kinetic and isotherm with linear and non-linear mathematical analysis. Surf Interfaces 20: 100616. https://doi.org/10.1016/j.surfin.2020.100616

Ghanim B, O'Dwyer TF, Leahy JJ, Willquist K, Courtney R, Pembroke JT, Murnane JG (2020) Application of KOH modified seaweed hydrochar as a biosorbent of vanadium from aqueous solution: characterisations, mechanisms and regeneration capacity. J Environ Chem Eng 8:104176. https://doi.org/10.1016/j.jece.2020.104176

Ghasemi Torkabad M, Keshtkar AR, Safdari SJ (2017) Comparison of polyethersulfone and polyamide nanofiltration membranes for uranium removal from aqueous solution. Prog Nucl Energy 94:93–100. https://doi.org/10.1016/j.pnucene.2016.10.005

Guo X, Liu Q, Liu J, Zhang H, Yu J, Chen R, Song D, Li R, Wang J (2019) Magnetic metal-organic frameworks/carbon dots as a multifunctional platform for detection and removal of uranium. Appl Surf Sci 491:640–649. https://doi.org/10.1016/j.apsusc.2019.06.108

Hassani S, Shirani M, Semnani A, Hassani M, Firooz A (2017) Removal of Congo red by magnetic nano-alumina using response surface methodology and artificial neural network. Desalination Water Treat 62:241–251. https://doi.org/10.5004/dwt.2017.0018

Huang Y, Zheng H, Li H, Zhao C, Zhao R, Li S (2020) Highly selective uranium adsorption on 2-phosphonobutane-1,2,4-tricarboxylic acid-decorated chitosan-coated magnetic silica nanoparticles. Chem Eng J 388:124349. https://doi.org/10.1016/j.cej.2020.124349

Ishag A, Li Y, Zhang N, Wang H, Guo H, Mei P, Sun Y (2020) Environmental application of emerging zero-valent iron-based materials on removal of radionuclides from the wastewater: a review. Environ Res 188:109855. https://doi.org/10.1016/j.envres.2020.109855

Leon CAL, Solar JM, Calemma V, Radovic LR (1992) Evidence for the protonation of basal plane sites on carbon. Carbon 30:797–811. https://doi.org/10.1016/0008-6223(92)90164-R

Li B, Hu J, Xiong H, Xiao Y (2020a) Application and properties of microporous carbons activated by ZnCl2: adsorption behavior and activation mechanism. ACS Omega 5:9398–9407. https://doi.org/10.1021/acsomega.0c00461

Li F-F, Cui W-R, Jiang W, Zhang C-R, Liang R-P, Qiu J-D (2020b) Stable sp2 carbon-conjugated covalent organic framework for detection and efficient adsorption of uranium from radioactive wastewater. J Hazard Mater 392:122333. https://doi.org/10.1016/j.jhazmat.2020.122333

Liew RK, Chong MY, Osazuwa OU, Nam WL, Phang XY, Su MH, Cheng CK, Chong CT, Lam SS (2018) Production of activated carbon as catalyst support by microwave pyrolysis of palm kernel shell: a comparative study of chemical versus physical activation. Res Chem Intermed 44:3849–3865. https://doi.org/10.1007/s11164-018-3388-y

Liu C, Dong Z, Yu C, Gong J, Wang Y, Zhang Z, Liu Y (2021a) Study on photocatalytic performance of hexagonal SnS2/g-C3N4 nanosheets and its application to reduce U(VI) in sunlight. Appl Surf Sci 537: 147754. https://doi.org/10.1016/j.apsusc.2020.147754

Liu Y, Huo Y, Wang X, Yu S, Ai Y, Chen Z, Zhang P, Chen L, Song G, Alharbi NS (2021b) Impact of metal ions and organic ligands on uranium removal properties by zeolitic imidazolate framework materials. J Clean Prod 278:123216. https://doi.org/10.1016/j.jclepro.2020.123216

Lu X, Zhang D, Tesfay Reda A, Liu C, Yang Z, Guo S, Xiao S, Ouyang Y (2017) Synthesis of amidoxime-grafted activated carbon fibers for efficient recovery of uranium(VI) from aqueous solution. Ind Eng

Chem Res 56:11936–11947. https://doi.org/10.1021/acs.iecr.7b02690
Mahmoud ME, Khalifa MA, El Wakeel YM, Header MS, Abdel-Fattah TM (2017) Engineered nano-magnetic iron oxide-urea-activated carbon nanolayer sorbent for potential removal of uranium (VI) from aqueous solution. J Nucl Mater 487:13–22. https://doi.org/10.1016/j.jnucmat.2017.01.046
Marciniak M, Goscianska J, Pietrzak R (2018) Physicochemical characterization of ordered mesoporous carbons functionalized by wet oxidation. J Mater Sci 53:5997–6007. https://doi.org/10.1007/s10853-017-1960-2
Marsh H, Reinoso FR (2006) Activated carbon. Elsevier
Marsh H, Yan DS, O'Grady TM, Wennerberg A (1984) Formation of active carbons from cokes using potassium hydroxide Carbon 22: 603-611. https://doi.org/10.1016/0008-6223(84)90096-4
Mokhine ND, Mathuthu M, Stassen E (2020) Recovery of uranium from residue generated during Mo-99 production, using organic solvent extraction. Phys Chem Earth, Parts A/B/C 115:102822. https://doi.org/10.1016/j.pce.2019.102822
Mullick A, Moulik S, Bhattacharjee S (2018) Removal of hexavalent chromium from aqueous solutions by low-cost rice husk-based activated carbon: kinetic and thermodynamic studies. Indian Chem Eng 60:58–71. https://doi.org/10.1080/00194506.2017.1288173
Naderi P, Shirani M, Semnani A, Goli A (2018) Efficient removal of crystal violet from aqueous solutions with Centaurea stem as a novel biodegradable bioadsorbent using response surface methodology and simulated annealing: kinetic, isotherm and thermodynamic studies. Ecotoxicol Environ Saf 163:372–381. https://doi.org/10.1016/j.ecoenv.2018.07.091
Nnadozie EC, Ajibade PA (2020) Data for experimental and calculated values of the adsorption of Pb(II) and Cr(VI) on APTES functionalized magnetite biochar using Langmuir, Freundlich and Temkin equations. Data Brief 32:106292. https://doi.org/10.1016/j.dib.2020.106292
Om Prakash M, Raghavendra G, Ojha S, Panchal M (2021) Characterization of porous activated carbon prepared from arhar stalks by single step chemical activation method. Mater Today Proc 39:1476–1481. https://doi.org/10.1016/j.matpr.2020.05.370
Qu J, Liu Y, Cheng L, Jiang Z, Zhang G, Deng F, Wang L, Han W, Zhang Y (2021) Green synthesis of hydrophilic activated carbon supported sulfide nZVI for enhanced Pb(II) scavenging from water: characterization, kinetics, isotherms and mechanisms. J Hazard Mater 403:123607. https://doi.org/10.1016/j.jhazmat.2020.123607
Ribeiro C, Scheufele FB, Espinoza-Quiñones FR, Módenes AN, Vieira MGA, Kroumov AD, Borba CE (2018) A comprehensive evaluation of heavy metals removal from battery industry wastewaters by applying bio-residue, mineral and commercial adsorbent materials. J Mater Sci 53:7976–7995. https://doi.org/10.1007/s10853-018-2150-6
Saleh TA, Naeemullah TM, Sarı A (2017) Polyethylenimine modified activated carbon as novel magnetic adsorbent for the removal of uranium from aqueous solution. Chem Eng Res Des 117:218–227. https://doi.org/10.1016/j.cherd.2016.10.030
Saputra A, Swantomo D, Ariyanto T, Sulistyo H (2019) Uranium removal from wastewater using Mg(OH)2-impregnated activated carbon. Water Air Soil Pollut 230:213. https://doi.org/10.1007/s11270-019-4269-8
Song S, Wang K, Zhang Y, Wang Y, Zhang C, Wang X, Zhang R, Chen J, Wen T, Wang X (2019) Self-assembly of graphene oxide/PEDOT:PSS nanocomposite as a novel adsorbent for uranium immobilization from wastewater. Environ Pollut 250:196–205. https://doi.org/10.1016/j.envpol.2019.04.020
Suárez L, Centeno TA (2020) Unravelling the volumetric performance of activated carbons from biomass wastes in supercapacitors. J Power Sources 448:227413. https://doi.org/10.1016/j.jpowsour.2019.227413
Taha MH, El-Maadawy MM, Hussein AEM, Youssef WM (2018) Uranium sorption from commercial phosphoric acid using kaolinite and metakaolinite. J Radioanal Nucl Chem 317:685–699. https://doi.org/10.1007/s10967-018-5951-9
Tan Y, Li L, Zhang H, Ding D, Dai Z, Xue J, Liu J, Hu N, Wang Y (2018) Adsorption and recovery of U(VI) from actual acid radioactive wastewater with low uranium concentration using thioacetamide modified activated carbon from liquorice residue. J Radioanal Nucl Chem 317: 811–824. https://doi.org/10.1007/s10967-018-5952-8
Tsai W-T, Bai Y-C, Lin Y-Q, Lai Y-C, Tsai C-H (2020) Porous and adsorption properties of activated carbon prepared from cocoa pod husk by chemical activation. Biomass Conv Bioref 10:35–43. https://doi.org/10.1007/s13399-019-00403-7
Wang C, Huang D, He F, Jin T, Huang B, Xu J, Qian Y (2020) Efficient removal of uranium(VI) from aqueous solutions by triethylenetetramine-functionalized single-walled carbon nanohorns. ACS Omega 5:27789–27799. https://doi.org/10.1021/acsomega.0c02715
Wazir AH, Haq I, Manan A, Khan A (2020) Preparation and characterization of activated carbon from coal by chemical activation with KOH. Int J Coal Prep Util:1–12. https://doi.org/10.1080/19392699.2020.1727896
Wu Q, Lv H, Zhao L (2020) Applications of carbon nanomaterials in chiral separation. TrAC Trends Anal Chem 129:115941. https://doi.org/10.1016/j.trac.2020.115941
Yagmur E, Gokce Y, Tekin S, Semerci NI, Aktas Z (2020) Characteristics and comparison of activated carbons prepared from oleaster (Elaeagnus angustifolia L.) fruit using KOH and ZnCl2. Fuel 267:117232. https://doi.org/10.1016/j.fuel.2020.117232
Yi Z, Liu J, Zeng R, Liu X, Long J, Huang B (2020) Removal of uranium(VI) from aqueous solution by Camellia oleifera shell-based activated carbon: adsorption equilibrium, kinetics, and thermodynamics. Water Sci Technol 82:2592–2602. https://doi.org/10.2166/wst.2020.504
Yildirim A, Baran MF, Acay H (2020) Kinetic and isotherm investigation into the removal of heavy metals using a fungal-extract-based bionanosorbent. Environ Technol Innov 20:101076. https://doi.org/10.1016/j.eti.2020.101076
Zahran F, El-Maghrabi HH, Hussein G, Abdelmaged SM (2019) Fabrication of bentonite based nanocomposite as a novel low cost adsorbent for uranium ion removal. Environ Nanotechnol Monit Manag 11:100205. https://doi.org/10.1016/j.enmm.2018.100205
Zhang C, Li X, Chen Z, Wen T, Huang S, Hayat T, Alsaedi A, Wang X (2018) Synthesis of ordered mesoporous carbonaceous materials and their highly efficient capture of uranium from solutions. Sci China Chem 61:281–293. https://doi.org/10.1007/s11426-017-9132-7
Zhang J, Chen X, Zhou J, Luo X (2020a) Uranium biosorption mechanism model of protonated Saccharomyces cerevisiae. J Hazard Mater 385:121588. https://doi.org/10.1016/j.jhazmat.2019.121588
Zhang M, Yuan M, Zhang M, Wang M, Chen J, Li R, Qiu L, Feng X, Hu J, Wu G (2020b) Efficient removal of uranium from diluted aqueous solution with hydroxypyridone functionalized polyethylene nonwoven fabrics. Radiat Phys Chem 171:108742. https://doi.org/10.1016/j.radphyschem.2020.108742
Zhong X, Liang W, Wang H, Xue C, Hu B (2021) Aluminum-based metal-organic frameworks (CAU-1) highly efficient UO22+ and TcO4− ions immobilization from aqueous solution. J Hazard Mater 407:124729. https://doi.org/10.1016/j.jhazmat.2020.124729
Zhuang S, Wang J (2020) Poly amidoxime functionalized carbon nanotube as an efficient adsorbent for removal of uranium from aqueous solution. J Mol Liq 319:114288. https://doi.org/10.1016/j.molliq.2020.114288